

## Pump-coupled high- $Q$ micromasers with conditional measurements of atoms: Transient and steady-state entanglement of nonlocal fields

Pál Bogár, János A. Bergou, and Mark Hillery

*Department of Physics and Astronomy, Hunter College of the City University of New York,  
695 Park Avenue, New York, New York, 10021*

(Received 1 July 1994; revised manuscript received 28 September 1994)

Two lossless micromasers are coupled in a series by the common pumping beam of two-level atoms the states of which are measured conditionally after the second cavity. Pure evolutions of the two fields are studied starting from uncorrelated coherent states for the four measurement schemes denoted by  $a-M'M''-a$ ,  $b-M'M''-b$ ,  $a-M'M''-b$ , and  $b-M'M''-a$  indicating the state of each atom,  $|a\rangle$  or  $|b\rangle$ , before and after the two maser cavities,  $M'$  and  $M''$ . It is shown that energy-preserving schemes (first two above) produce a two-dimensional set of distinct Fock states at a steady state under the envelope of the initial amplitude distribution of the fields. Since the initial fields were uncorrelated the generated ones will be uncorrelated, too. In the case of energy-transferring schemes (second two) the system makes transitions between correlated and uncorrelated regimes. Nonlocal superpositions reminiscent of the form of  $|N, N+M\rangle + |N+M, N\rangle$  can be generated at an optimum number of atoms as a result of two coexisting trapping mechanisms. This is a transient entanglement since it is destroyed by the atoms to follow due to the trapping effects themselves. However, we also show that by switching from any of the two energy-transferring schemes to any of the two preserving ones the transient correlation produced by the former scheme can be frozen into a steady state by the latter one. In the absence of dissipations this combination of schemes can generate steady-state coherent superpositions of arbitrary number states of two nonlocal fields (nonlocal Schrödinger cats) at reasonably high detection probabilities of the conditioned atomic states.

PACS number(s): 42.50.Dv, 42.52.+x

### I. INTRODUCTION

It has been shown that the one-atom maser [1], or micromaser is a genuine quantum device. The interaction of its single-mode microwave field in a high- $Q$  cavity with the driving two-level Rydberg atoms illustrates the irreconcilable difference between classical and quantum physics particularly clearly [2,3]. Nonclassical states of the radiation field were shown to be created in this system theoretically [4–17] and successfully generated experimentally [18–22]. There has always been a satisfactory agreement between experimental data and theoretical predictions.

One way to prepare such nonclassical fields is to perform measurements [23–25] on the atoms emerging from the interaction cavity making the field part of the entangled atom-field system reduce into the desired quantum state. The outcome of the measurements is not totally predictable, since according to quantum mechanics there is an element of chance attached to it. Nevertheless, a certain sequence of measurements determines the state of the field completely. In other words, we do not know prior to the experiment which state of the field will be produced, but we can redo the experiment until the required sequence of measurements, consequently the desired trajectory for the evolution of the state of the field, is achieved. This is called conditional measurement.

In this paper we couple two micromasers in series via the common pumping atomic beam [26] and perform conditional measurements on the state of the atoms em-

erging from the second micromaser (see Fig. 1). We consider four different measurement schemes: when the first micromaser is pumped by atoms in the upper (or lower) state of the maser transition and each of them emerging from the second micromaser is required to be detected in the upper (or lower) state in a row. Let us denote these schemes by  $a-M'M''-a$ ,  $b-M'M''-b$ ,  $a-M'M''-b$ , and  $b-M'M''-a$  showing the state of each atom,  $|a\rangle$  or  $|b\rangle$ , before and after the interaction with the two maser cavities,  $M'$  and  $M''$ . The following assumptions are applied.

First, there is at most one atom present in the cavities at a time in order to avoid cooperative effects. This is the usual regime in which the one-atom maser experiments operate. As a second condition, we consider extremely high- $Q$  cavities, where the loss of photons during the time of the experiment can be ignored. The quality factor  $Q$  of the cavities can reach values of up to  $10^{11}$ , and with a mi-

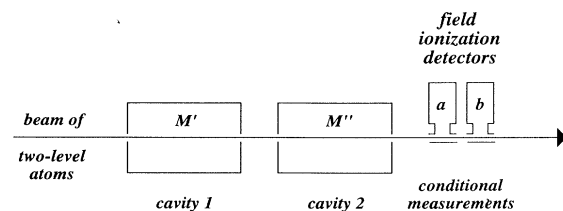


FIG. 1. Schematic arrangement of two micromasers coupled by a beam of two-level atoms the state of which is measured after the interaction.

crowave frequency of 20 GHz this results in photon lifetimes of several seconds. Third, thermal photons also have to be suppressed in order to avoid the induced decay of the fields. We can eliminate thermal photons by cooling the cavities down to a temperature of  $T=0.1$  K and the corresponding mean photon number at the above microwave frequency is  $3 \times 10^{-5}$ . Finally, we assume 100% detection efficiency for the field-ionization detectors measuring the state of the outgoing atoms in order to have each atom detected after the interaction.

By the time the atoms reach the second cavity they have gone through an interaction with the first field. The second micromaser is consequently pumped by atoms in a coherent superposition of their two masing levels depending upon the state of the field in the first one. In other words, there are always two different paths that the atoms can follow to reach the same final state detected, the probabilities of which depend upon the state of the field in the first micromaser. Quantum coherence, i.e., quantum correlation between the two fields arises from the interference of the two atomic paths, reminiscent of the one in Young's double slit experiment [26]. As soon as we have "which-path" information, i.e., the state of the atom between the cavities is detected, the coherence disappears. In the absence of losses we can use the wave function of the entangled system of the two fields because pure quantum states are achieved. The effect of losses and thermal radiation mixing the quantum states of the fields is investigated in a subsequent publication. It is shown there that coherence survives these decay processes and manifests itself in a typical structure of the density matrix indicating the two different atomic paths.

The present paper studies the evolution of the pure quantum states of the composite system of the two fields for all four schemes described above. The probabilities of the two atomic paths are manipulated via the interaction times in the two cavities. For initial uncorrelated coherent states of the fields one can produce a two-dimensional set of uncorrelated Fock states using energy-preserving schemes, while in the case of energy-transferring schemes transient entanglement of the fields can be achieved. Combining the two kinds of schemes together we show that steady-state production of arbitrary coherent superpositions of macroscopically high photon number states of the two different micromaser fields—often referred to as nonlocal Schrödinger cats—can be generated [27,28].

The paper is organized as follows. Section II reviews the single lossless micromaser problem with conditional measurements in order to see the effect of measurement and to set up a notation. Section III introduces the corresponding two-cavity problem the results of which are then used to investigate the four above mentioned measurement schemes and their combinations in Sec. IV. Section V is devoted to discussions and summary.

## II. SINGLE MICROMASER WITH CONDITIONAL MEASUREMENTS OF ATOMS

Consider a beam of two-level atoms (upper  $|a\rangle$ , lower  $|b\rangle$ ) interacting with a resonant microwave field in a loss-

less cavity of zero temperature. Atoms are consecutively injected in such a way that there is at most one atom in the cavity at a time, and the interaction time is the same for each atom (i.e., no atomic velocity spread). We know the state of the injected atoms before and measure the state of the outgoing atoms after the interaction. Let us consider four different schemes: each atom is injected in its upper (lower) state and detected in its upper (lower) state in a row. Let us denote these cases by:  $a$ - $M$ - $a$ ,  $b$ - $M$ - $b$ ,  $a$ - $M$ - $b$ , and  $b$ - $M$ - $a$ , showing the state of the atoms before and after the maser cavity,  $M$ .

The state of the field after the  $(k-1)$ th atom left but before the  $k$ th atom entered the cavity is given by

$$|\Psi^{(k-1)}\rangle = \sum_n \Psi_n^{(k-1)} |n\rangle. \quad (2.1)$$

After the interaction the state of the atom-field system reads as

$$|\Phi^{(k)}\rangle = \sum_n \Psi_n^{(k-1)} [C_{n+1} |a, n\rangle - iS_{n+1} |b, n+1\rangle], \quad (2.2a)$$

or

$$|\Phi^{(k)}\rangle = \sum_n \Psi_n^{(k-1)} [C_n |b, n\rangle - iS_n |a, n-1\rangle], \quad (2.2b)$$

if atom number  $k$  was injected in its upper, or lower state, respectively. Here  $C_n \equiv \cos(g\tau\sqrt{n})$  and  $S_n \equiv \sin(g\tau\sqrt{n})$ , where  $g$  is the atom-field coupling constant and  $\tau$  is the interaction time assumed to be the same for each atom.

Now, let us make a state measurement on the  $k$ th atom coming out from the cavity and consequently reduce the state of the field to

$$|\Psi^{(k)}\rangle = N^{(k)} \sum_n \Psi_n^{(k)} |n\rangle, \quad (2.3)$$

where  $N^{(k)}$  is the normalization constant and  $\Psi_n^{(k)}$  are the new amplitudes. Each measurement step is followed by the normalization of the state vector by  $N^{(k)}$ . The new amplitudes,  $\Psi_n^{(k)}$ , are functions of the old ones,  $\Psi_n^{(k-1)}$ , and for our four schemes they read as follows:

$$\Psi_n^{(k)} = \Psi_n^{(k-1)} C_{n+1}, \quad (2.4a)$$

$$\Psi_n^{(k)} = \Psi_n^{(k-1)} C_n, \quad (2.4b)$$

$$\Psi_n^{(k)} = \Psi_{n-1}^{(k-1)} S_n, \quad (2.4c)$$

$$\Psi_n^{(k)} = \Psi_{n+1}^{(k-1)} S_{n+1}, \quad (2.4d)$$

for the schemes  $a$ - $M$ - $a$ ,  $b$ - $M$ - $b$ ,  $a$ - $M$ - $b$ , and  $b$ - $M$ - $a$ , respectively, providing us with the iteration rules to determine the evolution of the state of the fields from atom to atom. The probability of finding the  $k$ th atom in the desired state is calculated as

$$P^{(k)} = \sum_n |\Psi_n^{(k)}|^2 = \frac{1}{N^{(k)2}}. \quad (2.5)$$

Starting from an initial field given by the amplitudes,  $\Psi_n^{(0)}$ , apart from the normalization constant the field amplitudes after the  $k$ th atom are given by

$$\Psi_n^{(k)} = \Psi_n^{(0)} C_{n+1}^k, \quad (2.6a)$$

$$\Psi_n^{(k)} = \Psi_n^{(0)} C_n^k, \quad (2.6b)$$

$$\Psi_n^{(k)} = \Psi_{n-k}^{(0)} S_n S_{n-1} \cdots S_{n-(k-1)}, \quad (2.6c)$$

$$\Psi_n^{(k)} = \Psi_{n+k}^{(0)} S_{n+1} S_{n+2} \cdots S_{n+k} \quad (2.6d)$$

for  $a$ - $M$ - $a$ ,  $b$ - $M$ - $b$ ,  $a$ - $M$ - $b$ , and  $b$ - $M$ - $a$ , respectively.

In the case of the two energy-preserving schemes,  $a$ - $M$ - $a$  and  $b$ - $M$ - $b$ , where atoms are injected and detected in the same states [29] it can be seen from Eqs. (2.6a) and (2.6b) that starting from, e.g., a coherent state of average photon number,  $|\alpha|^2$ , the state vector evolves toward one or a superposition of several distinct Fock states as atoms go through the cavity. (For the sake of simplicity we are going to use the term ‘‘Fock state’’ for the states that are actually Fock states only in the limit of  $k$  goes to infinity.) These peaks arise under the envelope of the initial amplitude distribution at those  $n$ 's where the cosine function is equal to zero in the limit of  $k$  goes to infinity. This means that the possible location of the peaks is determined by the equation,  $g\tau\sqrt{n+1}=l\pi$  for  $a$ - $M$ - $a$  and  $g\tau\sqrt{n}=l\pi$  for  $b$ - $M$ - $b$ , where  $l=0, 1, 2, \dots$ . Figure 2 gives two examples for  $a$ - $M$ - $a$  for an initial coherent state of average photon number,  $\alpha^2=10$ , atom number,  $k=100$ , and interaction parameters,  $g\tau=1.0$  and  $\pi$ . A single Fock state,  $|9\rangle$ , and a superposition of Fock states at integer's squares minus one are generated for  $g\tau=1.0$  and  $\pi$ , respectively. We get very similar results for  $b$ - $M$ - $b$ , although the peaks are shifted exactly by one toward larger  $n$ 's for the  $+1$  difference in the argument of the cosine functions in Eqs. (2.6a) and (2.6b). For later purposes we should mention here that for this reason it is possible to generate the vacuum Fock state,  $|0\rangle$ , via  $b$ - $M$ - $b$  which is not possible via  $a$ - $M$ - $a$ . The physical meaning of the  $+1$  is that a two-level atom cannot absorb a photon from, but can emit a photon to the vacuum. Apart from this difference these two schemes apply very similar mechanisms. The measurement process favors those photon numbers for which the Rabi angle is close to the multiples of  $\pi$  in order to have the same atomic state detected as the one that was injected. The state vector gradually becomes peaked at these photon numbers as atoms pass through.

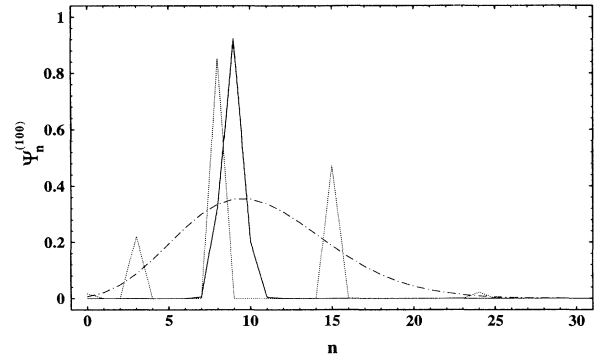


FIG. 2. Amplitude distribution in the number representation of the state vector of the field in a single micromaser in the case of scheme  $a$ - $M$ - $a$ . The dot-dashed line represents the initial coherent field of parameter  $\alpha^2=10$ . The fields generated at atom number  $k=100$  for  $g\tau=1.0$  and  $\pi$  are depicted by the solid and dotted lines, respectively.

For the energy-transferring schemes,  $a$ - $M$ - $b$  and  $b$ - $M$ - $a$ , where atoms are injected and detected in different states, we have a complicated product of different sine functions in Eqs. (2.6c) and (2.6d). The example depicted in Fig. 3 for  $a$ - $M$ - $b$  shows that the initial distribution of the coherent states separates into two distinct parts as atoms pass through. The iteration rule Eq. (2.4c) tells us that the state vector shifts by one photon and gets multiplied by the same sine function,  $S_n$ , every time an atom passes through. Hence, a growing region of the state vector will have zero amplitudes when multiplied by  $S_n=0$ , until finally, at a certain atom number  $k$  the whole wave function becomes zero. For this and all the consecutive atoms the probability of measuring the desired atomic state,  $|b\rangle$ , is zero. The atom is trapped in the other state,  $|a\rangle$ , and the conditional measurement scheme cannot be followed beyond this point. If there is no such integer number  $n$  for which  $S_n=0$  exactly, we will end up with a rapidly oscillating amplitude distribution as can be seen in the figure enlarged due to the disappearance of the regular peaks evolving toward larger photon numbers (in  $a$ - $M$ - $b$  atoms always leave a photon in the cavity). Although the probability of detecting the lower atomic state

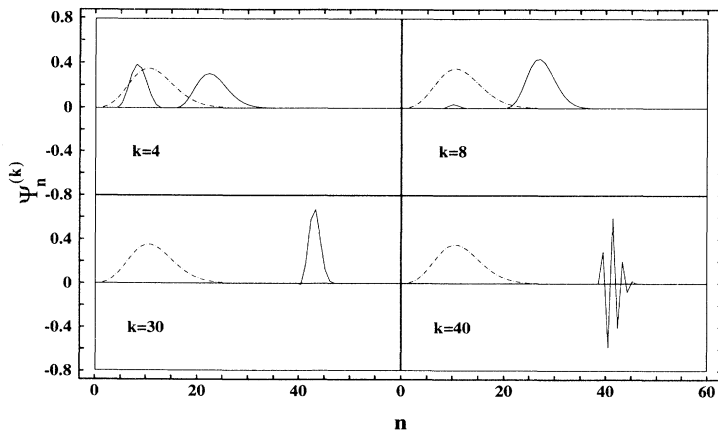


FIG. 3. Amplitude distribution in the number representation of the state vector of the field in a single micromaser in the case of scheme  $a$ - $M$ - $b$ . The dot-dashed lines represent the initial coherent field of parameter  $\alpha^2=10$  and the fields generated at different atom numbers  $k=4, 8, 30$  and  $40$  for  $g\tau=0.9$  are depicted by the solid lines.

is not zero in this case but it is small. The largest separation of the regular peaks that can be achieved before trapping (or before the oscillatory structure would show up) is determined by the location of the trapping states for which  $S_{n_l} = 0$ , given by  $n_l = (l\pi/g\tau)^2$ ,  $l=1,2,3,\dots$

The distribution is bound to evolve between these boundaries. Apart from the  $+1$  difference in the argument of the sine functions in Eqs. (2.4c) and (2.4d) we have exactly the same effect for  $b$ - $M$ - $a$ , except that the direction of the shift in Eq. (2.4d) is the opposite, consequently, the peaks evolve toward lower  $n$ 's ending up finally in one of the trapping states after a certain number of atoms (in  $b$ - $M$ - $a$  atoms always absorb a photon from the cavity). Schemes,  $a$ - $M$ - $b$  and  $b$ - $M$ - $a$ , apply the same mechanisms. The measurement process suppresses those photon numbers from the distribution for which the Rabi angle is close to the multiples of  $\pi$  and the emission (absorption) of a photon is prohibited for  $a$ - $M$ - $b$  ( $b$ - $M$ - $a$ ). After a certain number of atoms the whole state vector becomes practically zero and the atoms are trapped in the upper (lower) state.

We are going to see the implications of these effects in the two-cavity problem in the next sections in "two degrees of freedom." The measurement process will select a pair or, more importantly, sometimes *two* pairs of photon numbers from the two fields to favor (disfavor). An in-

terference of the two corresponding paths is expected in the latter case indicating that the states of the fields in the two *separate* micromaser cavities are no longer independent but they are *correlated*.

### III. COUPLED MICROMASERS WITH CONDITIONAL MEASUREMENTS OF ATOMS

Let us consider now two micromaser fields coupled by the common pumping atomic beam in such a way that atoms first interact with the field in cavity 1 and then proceed to cavity 2 (see Fig. 1). The same assumptions apply as in Sec. II: no cavity losses, zero temperature, single atom resonant interaction, no atomic velocity spread, 100% detection efficiency. Similarly to Sec. II we investigate four different schemes:  $a$ - $M'$ - $M''$ - $a$ ,  $b$ - $M'$ - $M''$ - $b$ ,  $a$ - $M'$ - $M''$ - $b$ , and  $b$ - $M'$ - $M''$ - $a$  indicating the state of each atom,  $|a\rangle$  or  $|b\rangle$ , before and after the two maser cavities,  $M'$  and  $M''$ .

The state of the field after the  $(k-1)$ th atom left but before the  $k$ th atom entered the cavity is given by

$$|\Psi^{(k-1)}\rangle = \sum_{n_1, n_2} \Psi_{n_1, n_2}^{(k-1)} |n_1, n_2\rangle. \quad (3.1)$$

After the  $k$ th atom has interacted with the fields the state of the atom-fields system reads as

$$\begin{aligned} |\Phi^{(k)}\rangle = \sum_{n_1, n_2} \Psi_{n_1, n_2}^{(k-1)} [ & C'_{n_1+1} (C''_{n_2+1} |a, n_1, n_2\rangle - iS''_{n_2+1} |b, n_1, n_2+1\rangle) \\ & - iS'_{n_1+1} (C''_{n_2} |b, n_1+1, n_2\rangle - iS''_{n_2} |a, n_1+1, n_2-1\rangle) ], \end{aligned} \quad (3.2a)$$

or

$$\begin{aligned} |\Phi^{(k)}\rangle = \sum_{n_1, n_2} \Psi_{n_1, n_2}^{(k-1)} [ & C'_n (C''_{n_2} |b, n_1, n_2\rangle - iS''_{n_2} |a, n_1, n_2-1\rangle) \\ & - iS'_{n_1} (C''_{n_2+1} |a, n_1-1, n_2\rangle - iS''_{n_2+1} |b, n_1-1, n_2+1\rangle) ], \end{aligned} \quad (3.2b)$$

if the atom was injected in its upper, or lower state, respectively. Here,  $S'_{n_1} \equiv \sin(g'\tau'\sqrt{n_1})$  and  $C'_{n_1} \equiv \cos(g'\tau'\sqrt{n_1})$  correspond to the first and the double-primed ones,  $S''_{n_2}$  and  $C''_{n_2}$ , to the second micromaser. After the interaction with both fields the state of the atom is measured and the state of the fields is reduced to

$$|\Psi^{(k)}\rangle = N^{(k)} \sum_{n_1, n_2} \Psi_{n_1, n_2}^{(k)} |n_1, n_2\rangle. \quad (3.3)$$

Each measurement is followed by a renormalization of the state vector by  $N^{(k)}$ . The new amplitudes,  $\Psi_{n_1, n_2}^{(k)}$ , are functions of the old ones,  $\Psi_{n_1, n_2}^{(k-1)}$ , and for our four schemes they read as follows:

$$\Psi_{n_1, n_2}^{(k)} = \Psi_{n_1, n_2}^{(k-1)} C'_{n_1+1} C''_{n_2+1} - \Psi_{n_1-1, n_2+1}^{(k-1)} S'_{n_1} S''_{n_2+1}, \quad (3.4a)$$

$$\Psi_{n_1, n_2}^{(k)} = \Psi_{n_1, n_2}^{(k-1)} C'_{n_1} C''_{n_2} - \Psi_{n_1+1, n_2-1}^{(k-1)} S'_{n_1+1} S''_{n_2}, \quad (3.4b)$$

$$\Psi_{n_1, n_2}^{(k)} = \Psi_{n_1, n_2-1}^{(k-1)} C'_{n_1+1} S''_{n_2} + \Psi_{n_1-1, n_2}^{(k-1)} S'_{n_1} C''_{n_2}, \quad (3.4c)$$

$$\Psi_{n_1, n_2}^{(k)} = \Psi_{n_1, n_2+1}^{(k-1)} C'_{n_1} S''_{n_2+1} + \Psi_{n_1+1, n_2}^{(k-1)} S'_{n_1+1} C''_{n_2+1}, \quad (3.4d)$$

for  $a$ - $M'$ - $M''$ - $a$ ,  $b$ - $M'$ - $M''$ - $b$ ,  $a$ - $M'$ - $M''$ - $b$ , and  $b$ - $M'$ - $M''$ - $a$ , respectively, providing us with the iteration rules determining the evolution of the state of the fields from atom to atom. The probability of finding the  $k$ th atom in the desired state is

$$P^{(k)} = \sum_{n_1, n_2} |\Psi_{n_1, n_2}^{(k)}|^2 = \frac{1}{N^{(k)2}}. \quad (3.5)$$

The evolution of the two fields will be studied in the next section by iterating the amplitudes according to one of the rules above starting from coherent states of the two fields. We are going to investigate the correlations building up between the two micromasers as a result of the interference between the two paths that each atom can follow when traversing the cavities. In order to do so we define  $m$ th-order correlation by the nonseparability condition given by

$$\langle (\hat{a}_1 \hat{a}_2^\dagger)^m \rangle \neq \langle \hat{a}_1^m \rangle \langle \hat{a}_2^{\dagger m} \rangle, \quad (3.6)$$

where  $\hat{a}_1$  and  $\hat{a}_2$  are the field operators of micromasers 1 and 2, respectively. We would like to draw attention to that fact that this is a correlation between fields of two different micromasers, i.e., an entanglement of two *nonlocal* subsystems. Thus, carrying out a measurement that reduces the state of one of the fields results in a reduction of the state of the other field located at a different point in space. One example of such a state vector of  $M$ th-order correlation is given by

$$|\Psi\rangle = \frac{1}{\sqrt{2}}(|n_1, n_2\rangle \pm |n_1 \pm M, n_2 \mp M\rangle), \quad (3.7)$$

a possible production of which will be shown in the next section (see also in Ref. [28]).

#### IV. EVOLUTION OF THE FIELDS FOR VARIOUS CONDITIONAL MEASUREMENT SCHEMES

Let us assume that both field are initially in coherent states of the same  $\alpha$  given by

$$|\Psi^{(0)}\rangle = e^{-\alpha^2} \sum_{n_1, n_2} \frac{\alpha^{n_1+n_2}}{\sqrt{n_1!n_2!}} |n_1, n_2\rangle \quad (4.1)$$

depicted for  $\alpha^2=10$  and  $k=0$  in Fig. 5. According to Eq. (3.6) the two fields are uncorrelated because their state vector is separable into a tensor product of two coherent states in the two cavities  $|\alpha\rangle_{\text{cavity1}} \otimes |\alpha\rangle_{\text{cavity2}}$ . We are going to consider typical examples for the evolution of the fields for the four conditional measurement schemes,  $a$ - $M'$  $M''$ - $a$ ,  $b$ - $M'$  $M''$ - $b$ ,  $a$ - $M'$  $M''$ - $b$ , and  $b$ - $M'$  $M''$ - $a$ , applying the corresponding iteration rules of Eq. (3.4) and assuming equal interaction parameters,  $g\tau \equiv g'\tau' = g''\tau''$ , in both cavities.

##### A. Energy-preserving schemes, $a$ - $M'$ $M''$ - $a$ and $b$ - $M'$ $M''$ - $b$

Atoms are injected into the first cavity and detected after the second one in the same state. Let us consider scheme  $a$ - $M'$  $M''$ - $a$  first. The possible paths the atom can follow are  $a_0 a_1 a_2$  and  $a_0 b_1 a_2$  in Fig. 4. They both preserve the total energy of the two micromasers. Furthermore,  $a_0 a_1 a_2$  preserves the photon number in both cavities separately, while  $a_0 b_1 a_2$  make the photon num-

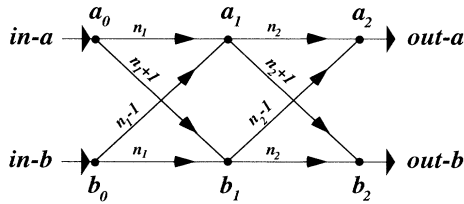


FIG. 4. Possible paths a two-level atom (upper  $a$ , lower  $b$ ) can follow when passing through the two micromaser fields. The indices 0, 1, and 2 represent the position of the atom before, between and after the two cavities, respectively. Starting from  $n_1$  and  $n_2$  the final number of photons due to each path is shown above the arrows.

ber increase in the first and decrease in the second cavity. We can manipulate the probabilities of these paths via the interaction times in the cavities. Let us see some typical examples for the evolution and the steady state of the fields at different parameters.

Consider the interaction parameter,  $g\tau=1.0$ . Figure 5 shows that the state of the fields gets localized approximately in the Fock state,  $|9,9\rangle$ , as atom number  $k$  goes to infinity, with some contributions from  $|10,8\rangle, |11,7\rangle, \dots, |18,0\rangle$  that are decreasing with  $k$ . The solid line in Fig. 7 shows that the probability of finding the atom in the required upper state is increasing with  $k$  and is approximately unity for large  $k$ 's. This effect can be understood in the following way. The initial amplitudes of the coherent fields are the largest around  $n_1=n_2=10$ . For these photon numbers and for the above interaction times the probability of path  $a_0 a_1 a_2$  is much larger than the one for the alternative path  $a_0 b_1 a_2$ , because  $C_{10} \cong 1$  and  $S_{10} \cong 0$  [see Eqs. (2.2a) and (2.2b)]. The fields get localized around  $n_1 \cong n_2 \cong 9$  due to path  $a_0 a_1 a_2$  corresponding to a Rabi angle of  $\pi$ , which localization further increases the enhancement of path  $a_0 a_1 a_2$  itself. Path  $a_0 b_1 a_2$  gives rise to the small contributions from  $|10,8\rangle, |11,7\rangle, \dots, |18,0\rangle$ . Apart from these small amplitudes this production of a Fock state is very similar to the one discussed in Sec. II for the case of the single micromaser. Since path  $a_0 a_1 a_2$  has a very high probability throughout the whole evolution all atoms are practically in their upper state before, between, and after the cavities. We practically have two *independent* micromasers both operating in scheme  $a$ - $M$ - $a$ , where atoms enter and leave both cavities in their upper state. Consequently, the same mechanism applies as the one for the single micromaser in  $a$ - $M$ - $a$  discussed in Sec. II, and we get the uncorrelated Fock state,  $|9,9\rangle$ , as a product of two  $|9\rangle$ 's depicted in Fig. 2 for each cavity. Small correlation builds up only in the transient regime of coexisting paths.

Let us now look at the interaction parameter,  $g\tau=0.5$ . Figure 6 shows the evolution of the state of the fields, while the probabilities of detecting the emerging atoms in the upper state are given by the dashed line in Fig. 7. For the initial coherent states the probability of path  $a_0 a_1 a_2$  is now much smaller than the one for  $a_0 b_1 a_2$ , which implies that the number of photons is initially increasing in cavity 1 and decreasing in cavity 2. This can be seen in Fig. 6 for  $k=10$  and 70. At around  $k=114$  the field in cavity 2 experiences a jump from vacuum to a high photon number, and finally the system settles to a Fock state around  $|39,39\rangle$  with some contributions from  $|40,38\rangle, |41,37\rangle, |42,36\rangle, \dots, |78,0\rangle$ . Since  $a_0 b_1 a_2$  has a high probability initially, atoms enter cavity 2 in their lower state. Thus cavity 1 operates in scheme  $a$ - $M$ - $b$  and cavity 2 in  $b$ - $M$ - $a$ . Due to the increasing photon number in cavity 1 this mechanism terminates itself according to the trapping effect in scheme  $a$ - $M$ - $b$  discussed in Sec. II. At  $n_1 \cong 39$  the probability of dropping a photon in cavity 1 becomes approximately zero, because  $S_{n_1+1} \cong 0$ , and the system is back to the schemes  $a$ - $M$ - $a, a$ - $M$ - $a$  in both cavities discussed above. The photon number in cavity 1

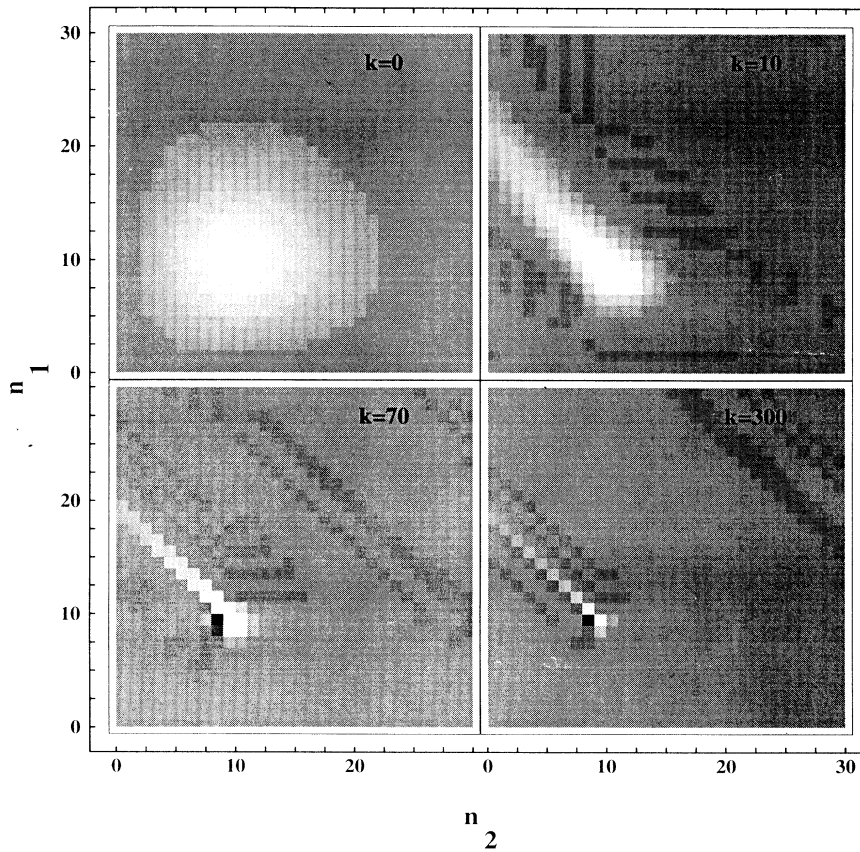


FIG. 5. Density plots showing the evolution of the amplitude distribution of the fields in the number representation in the case of scheme  $a$ - $M'M''$ - $a$ . Lighter and darker points indicate positive and negative amplitudes, respectively, as compared to the gray base of the zero level. The initial coherent field of parameter  $\alpha^2=10$  is given by the plot denoted by atom number  $k=0$ . The fields generated at  $g\tau=1.0$  for atom numbers  $k=10, 70$ , and  $300$  show a localization around the Fock state,  $|9,9\rangle$ , with small contributions from  $|10,8\rangle, |11,7\rangle, \dots, |18,0\rangle$  that are decreasing with  $k$ .

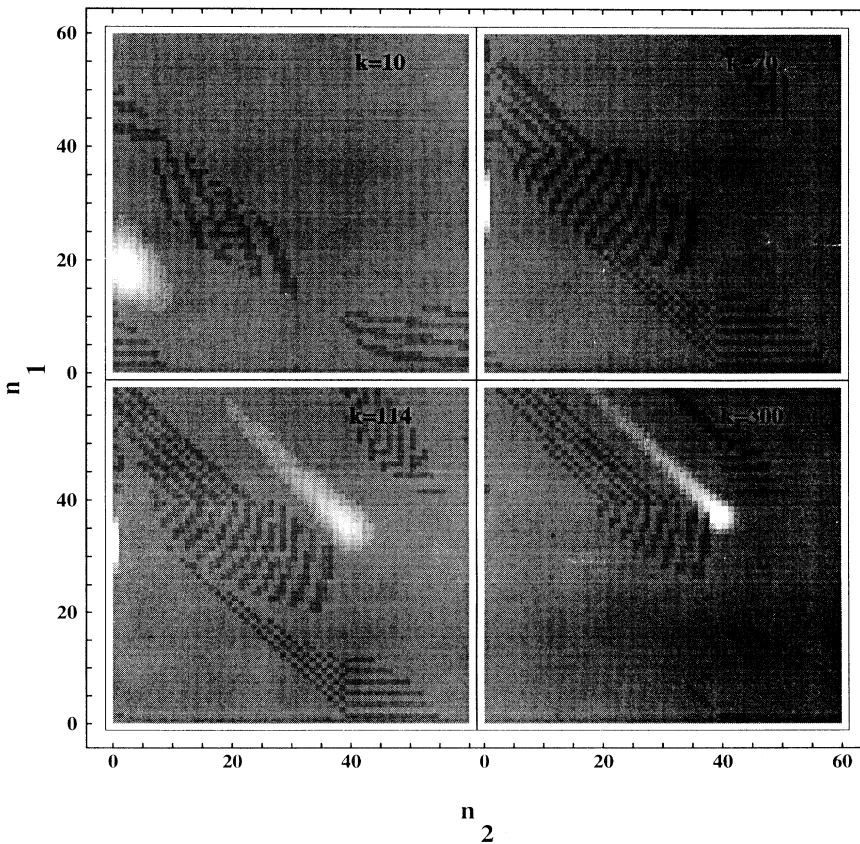


FIG. 6. Density plots showing the evolution of the amplitude distribution of the fields in scheme  $a$ - $M'M''$ - $a$  starting from the field shown in Fig. 5 for  $k=0$ . The generated fields at  $g\tau=0.5$  for atom numbers  $k=10, 70, 114$ , and  $300$  show a jump in the photon number in the second cavity around  $k=114$  and then a localization around the Fock state,  $|39,39\rangle$ , with small contributions from  $|40,38\rangle, |41,37\rangle, |42,36\rangle, \dots, |78,0\rangle$  that are decreasing with  $k$ .

locks to  $n_1 \cong 39$ , while the one in cavity 2 becomes peaked according to the mechanism in a single micromaser in scheme  $a$ - $M$ - $a$ . Thus, the same uncorrelated steady state of the fields is generated as if they were independent, but the time evolution is different. Both fields lock to photon numbers that assure a Rabi angle of  $\pi$  that implies an  $a$ - $M$ - $a$ ,  $a$ - $M$ - $a$  operation for both micromasers.

At large  $g\tau$ -s the system does not follow this kind of evolution (see Fig. 8). There are several photon numbers in this case that drive the atom into both atomic states between the cavities resulting in superimposed  $a$ - $M$ - $a$ ,  $a$ - $M$ - $b$  operation of the first and  $a$ - $M$ - $a$ ,  $b$ - $M$ - $a$  operation of the second micromaser. Nevertheless, the state of the fields at steady state settles to a superposition of Fock states in both cavities that assure Rabi angles that are the multiples of  $\pi$  resulting again in an indepen-

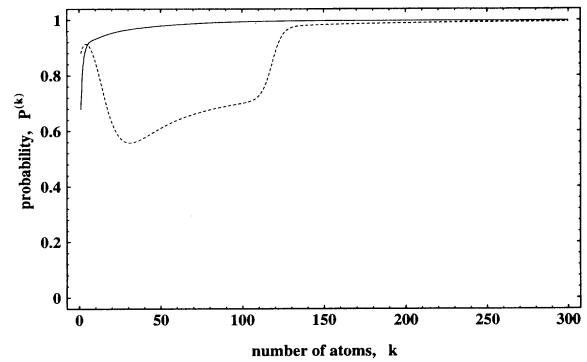


FIG. 7. The probabilities of detecting the upper state,  $|a\rangle$ , of atom number  $k$  in scheme  $a$ - $M'$  $M''$ - $a$  during the evolution of the fields shown in Figs. 5 and 6 for  $g\tau=1.0$  and  $0.5$  depicted by the solid and dashed lines, respectively.

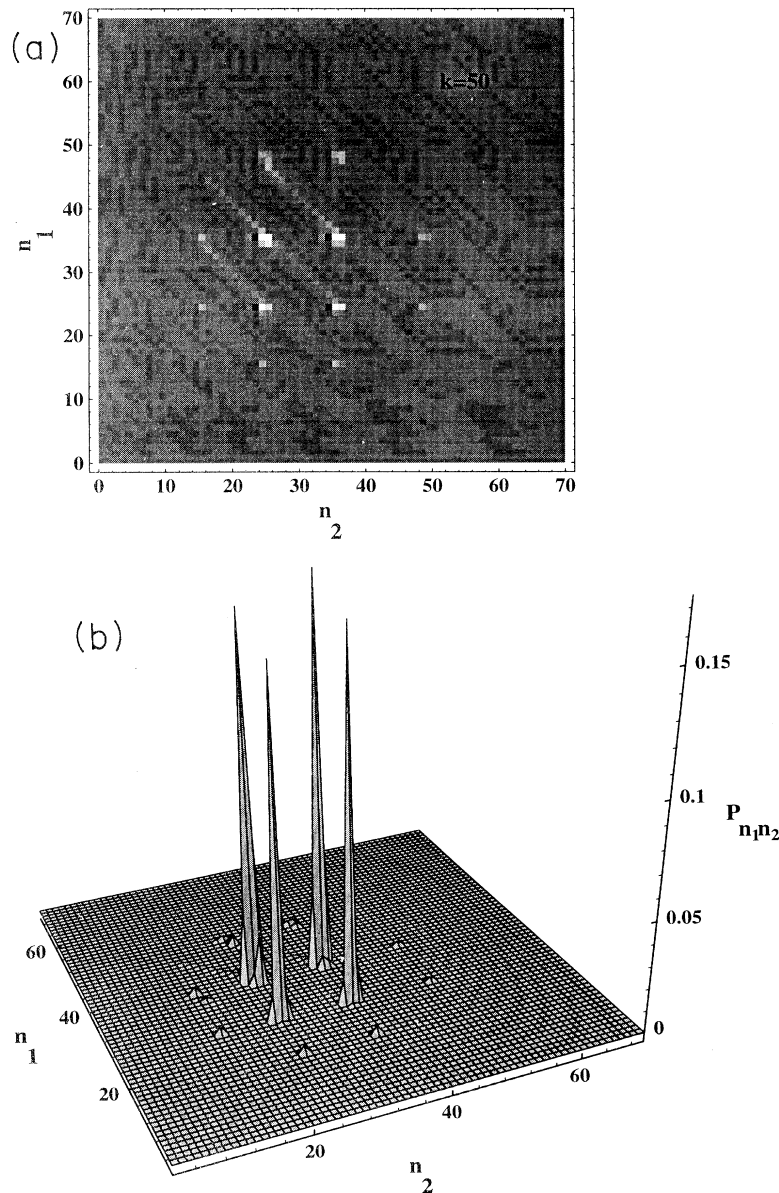


FIG. 8. (a) Density plot of the amplitude distribution of the fields in scheme  $a$ - $M'$  $M''$ - $a$  at atom number  $k=50$  for  $g\tau=\pi$  starting from coherent fields of parameter  $\alpha^2=30$ . The generated Fock states are located at photon numbers that are squares integers minus one under the envelope of the amplitude distribution of the initial fields. (b) Three-dimensional plot of the photon statistics that are the squares of the amplitudes depicted in (a).

dent  $a$ - $M$ - $a$ ,  $a$ - $M$ - $a$  operation for both micromasers. In the example in Fig. 8, where the parameter of the initial coherent state is  $\alpha^2=30$  and  $g\tau=\pi$  the fields settle to a steady-state superposition of Fock states at integer squares minus one, mainly at 24 and 35. Thus, the state of the field can be approximated with

$$|\Psi\rangle \cong N(|24, 24\rangle + |35, 35\rangle + |24, 35\rangle + |35, 24\rangle), \quad (4.2)$$

where  $N$  stands for normalization. It is easy to see that according to Eq. (3.6) the two fields are uncorrelated, because the state vector above is separable as

$$|\Psi\rangle \cong N(|24\rangle + |35\rangle)_{\text{cavity1}} \otimes (|24\rangle + |35\rangle)_{\text{cavity2}}. \quad (4.3)$$

In these examples for  $a$ - $M'$ - $M''$ - $a$  both micromasers operate at steady state in scheme  $a$ - $M$ - $a$ , i.e., from the possible paths  $a_0a_1a_2$  is realized only. The redistribution of the photons along path  $a_0b_1a_2$  changes the probabilities for the two paths in such a way that after a certain time evolution it will ultimately terminate itself. This will put both cavities into independent  $a$ - $M$ - $a$  schemes and atoms will go along  $a_0a_1a_2$  at steady state. Starting from uncorrelated coherent states of both fields there is a *transient entanglement* between them during the photon redistribution process until the steady state is reached. Due to the separability of the initial state the independent production of Fock states under the envelope of the initial amplitude distribution in the two cavities will also be separable providing us with fields that are *uncorrelated* at steady state as well.

Scheme  $b$ - $M'$ - $M''$ - $b$  is very similar to  $a$ - $M'$ - $M''$ - $a$  discussed above with some minor differences. First, there is a  $+1$  difference in the generated Fock states as a result of the  $+1$  difference in the arguments of the cosines in Eqs. (2.6a) and (2.6b) similarly to what we have seen in Sec. II. Second, it has also been shown there that due to this  $+1$  scheme  $b$ - $M$ - $b$  can while  $a$ - $M$ - $a$  cannot generate the vacuum. As a consequence of this the second field jumps to a vacuum in the case of scheme  $b$ - $M'$ - $M''$ - $b$  instead of the finite photon number that we have found above for  $a$ - $M'$ - $M''$ - $a$  at  $g\tau=0.5$ . Third, the opposite energy transfer between the cavities (the possible paths are  $b_0b_1b_2$  and  $b_0a_1b_2$ ) implies that the set of states contributing to the field additionally to the main Fock states is approximately the mirror image of the one in scheme  $a$ - $M'$ - $M''$ - $a$ . It follows that the degree of (transient) correlation is of the same order in both schemes.

In this subsection we considered the two energy preserving schemes,  $a$ - $M'$ - $M''$ - $a$  and  $b$ - $M'$ - $M''$ - $b$ , where the atoms are injected before and detected after the interaction to be in the same state. There are two possible paths they can follow: one which transports photons from one of the cavities to the other one and another which does not change the photon number at all. Only the latter one survives at steady state. The transporting path is transient and serves as a photon redistribution process to set the steady state of the fields in which it then terminates itself. Consequently, both micromasers are independently in the photon-preserving schemes,  $a$ - $M$ - $a$  or  $b$ - $M$ - $b$ , at steady state providing us with a set of Fock states assuring Rabi angles to be the multiples of

$\pi$  located under the envelope of the initial state of the fields. We want to emphasize here that only uncorrelated initial fields have been considered so far. It has been seen from the examples above that if the initial state of the fields were separable, then their steady state would be separate as well, i.e., uncorrelated initial fields provide us with uncorrelated steady-state fields. We are going to see in a later subsection that correlated initial fields result in correlated steady-state fields. We will show that an entanglement generated via some other schemes can be frozen into a steady state using one of the energy-preserving schemes,  $a$ - $M'$ - $M''$ - $a$ , or  $b$ - $M'$ - $M''$ - $b$ .

### B. Energy-transferring schemes, $a$ - $M'$ - $M''$ - $b$ and $b$ - $M'$ - $M''$ - $a$ , and two-cavity trapping

Atoms are injected into the first cavity and detected after the interaction in different states. Let us consider scheme  $a$ - $M'$ - $M''$ - $b$  first. The possible paths are  $a_0a_1b_2$  and  $a_0b_1b_2$  both increasing the energy of the system by one photon. The former one preserves the energy of the first and the latter one preserves the energy of the second micromaser.

Figure 9(a) shows typical evolution of the fields for short interaction times as in our example for  $g\tau=0.3, 0.5$ , and  $0.8$ . It can be seen in the first row of the figure for  $g\tau=0.3$  that since the probabilities of the two atomic paths are approximately equal at these interaction times for the dominant part of the initial field [ $C_{10} \cong S_{10}$  in Eqs. (2.2a) and (2.2b)] the amplitude distribution is stretched along a straight line as it is shown for  $k=20$ . It is easy to see that the state vector of the system cannot be separated into a product of two, consequently, the fields are correlated in this regime. In other words, due to the ‘‘optimum lack of which-path information’’ about the state of the atom between the cavities there is a strong interference between the two paths. The distribution, the shape of which becomes thinner as it evolves toward higher photon numbers (in the present scheme,  $a$ - $M'$ - $M''$ - $b$ , atoms are required to leave a photon in one of the two cavities), separates into two regions and finally ends up in a rapidly oscillating structure mainly around the vacuum of cavity 2 and  $n_1 \cong 50$  at  $k=40$ . The other region at the vacuum of cavity 1 and  $n_1 \cong 50$  has already disappeared. This effect cannot be explained by the single cavity trapping mechanism discussed in Sec. II since the formula  $n_l = (l\pi/g\tau)^2$  predicts a trapping for  $l=1$  at the photon number  $n_l \cong 100$  that is much higher than where the distribution is located in this example. We will explain later that this is due to a new mechanism that we call *two-cavity trapping* based on the coupling between the two fields to distinguish it from the *single-cavity trapping* discussed in Sec. II. In the second row for  $g\tau=0.5$  considering the dominant part of the initial field it is highly probable that the atom leaves a photon in cavity 1 [ $C_{10} \cong 0$  and  $S_{10} \cong 1$  in Eq. (2.2a)] making the second cavity operate in scheme  $b$ - $M$ - $b$ . Thus, the photon number increases in both cavities in such a way that the distribution localizes around a point in the  $n_1$ - $n_2$  space where  $n_1 \cong n_2$  showing a balance between the fields. The mechanism is very similar to the one for  $b$ - $M'$ - $M''$ - $b$  ex-

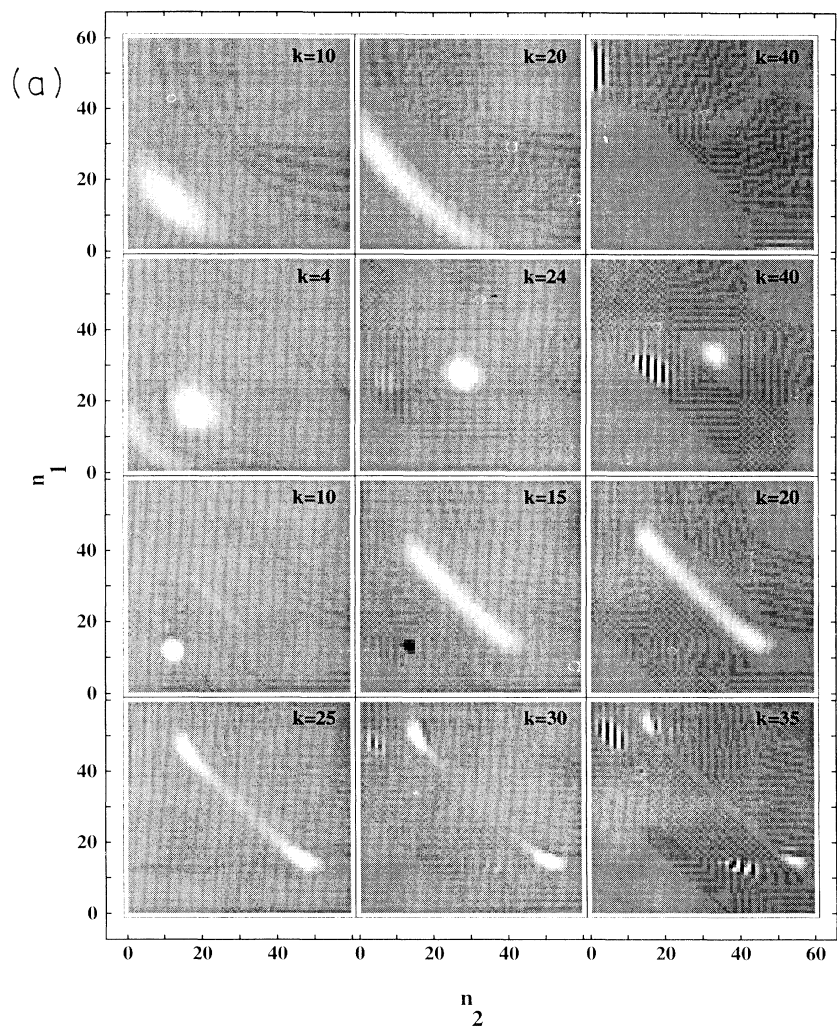
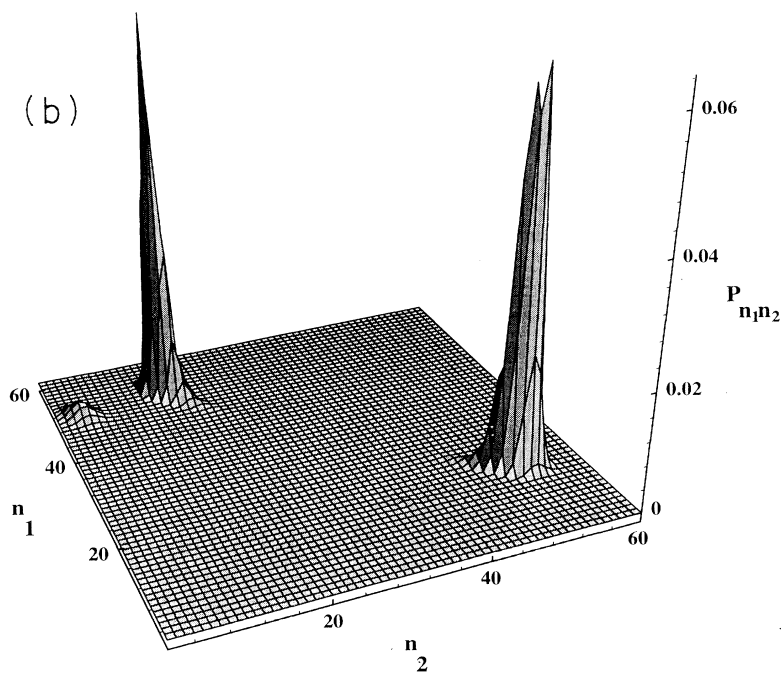


FIG. 9. (a) Density plots showing the evolution of the amplitude distribution of the fields in scheme  $a-M'M''-b$  starting from coherent fields depicted in Fig. 5 for  $k=0$ , where  $g\tau=0.3$  for the first, 0.5 for the second, and 0.8 for the third and fourth rows. The first and second rows represent the correlated and uncorrelated regimes, respectively, while a transition between these two regimes as well as a double-peaked distribution at  $k=30$  can be seen in the third and fourth ones. (b) Three-dimensional plot of the photon statistics that are the squares of the amplitudes depicted in (a) for  $g\tau=0.8$  at atom number  $k=30$  showing a double-peaked probability distribution.



cept now the distribution as a whole evolves toward higher photon numbers. Due to the localization, or in other words due to the “which-path” information that the atom is in its lower state between the cavities with high probability the two micromasers are uncorrelated in this regime. At  $n_1 \cong n_2 \cong 40$  the two fields independently reach their single-cavity trapping points determined by the formula  $n_l = (l\pi/g\tau)^2$  for  $l=1$ , where the oscillatory structure shows up exactly the same way as it has been discussed in Sec. II. The uncorrelated evolution ends up in an uncorrelated single-cavity trapping.

These two regimes shown in the first two rows of the figure are the basic mechanisms that the system follows. For larger interaction parameters, for example, for  $g\tau=0.8$  shown in the third and fourth rows of the figure, the system undergoes transitions between them. It can be seen in the third row that it switches from the uncorrelated regime to the correlated one at  $k=15$ . However, the stretched distribution evolving toward higher photon numbers experiences a new effect. It becomes double peaked around  $k=30$  showing fields with state vector approximately of the form of

$$|\Psi\rangle \cong N(|15, 50\rangle + |50, 15\rangle), \quad (4.4)$$

exhibiting, according to Eq. (3.6), 35th-order correlation ( $N$  is a normalization constant). This effect is similar to what happened to the distribution at  $g\tau=0.3$  and cannot be explained by the single-cavity trapping effect of Sec. II. The iteration rule given for the present scheme by Eq. (3.4c) tells us that the distribution separates into two parts as soon as it reaches  $n_1 \cong n_2 \cong 35$ . At these photon numbers and interaction parameters,  $g\tau=0.8$ , the cosines  $C_{n_1}$  and  $C_{n_2}$  become zero in the formula resulting in a zero amplitude for the middle of the stretched distribution. This zero amplitude region increases as atoms pass through due to the shift of the amplitudes from atom to atom in a similar way as discussed for the single-cavity trapping effect in Sec. II, except now it happens in two dimensions. This is a two-cavity trapping effect strongly relying on the coupling between the two fields, because it requires the cosines of both cavities  $C_{n_1}$  and  $C_{n_2}$  to be zero simultaneously in order to have both terms in the sum zero in Eq. (3.4c). Furthermore, it can be seen that since the amplitudes are shifted in both  $n_1$  and  $n_2$  in the equation the distribution will be suppressed in both directions of the  $n_1-n_2$  space. In the *single-cavity trapping* the sine function is zero resulting in trapped photon numbers at  $n_l = (l\pi/g\tau)^2, l=1, 2, 3, 4, \dots$ , while in the case of the *two-cavity trapping* the cosine function is zero implying  $n_{ll} = (l\pi/2g\tau)^2, l=1, 3, 5, \dots$ . Figure 9(a) shows that the double-peaked distribution built up by  $k=30$  begins to be destroyed at  $k=35$ . The two-cavity trapping suppresses the amplitudes starting from the middle, while the single-cavity trapping bounds the stretched distribution from the ends, showing the presence of the sine functions in the equation. These two mechanisms gradually suppress the state vector and finally result in the oscillatory structures as can be seen in the figure for  $k=35$ . In our example for  $g\tau=0.8$  the  $l=1$  single-cavity trapping lines are located at  $n_l \cong 15$  in both directions of  $n_1$  and  $n_2$

binding the stretched distribution from “outside.” The two-cavity trapping takes place when the middle of the distribution is at  $n_1 \cong n_2 \cong 35$ . These two mechanisms determine the location of the two peaks around  $n_1 \cong 15$  and 50 as well as  $n_2 \cong 50$  and 15 that can be approximated by Eq. (4.4). The photon statistics of the fields that are equal to the square of the amplitude distribution given in the density plots are shown in Fig. 9(b) for the double-peaked structure depicted in Fig. 9(a) for  $g\tau=0.8$ , and  $k=30$ . Similar explanation can be given for what we have seen in the case of  $g\tau=0.3$ .

The probabilities that the atoms are detected in their lower state after the interaction according to the scheme  $a-M'M''-b$  are depicted in Fig. 10 for the three examples of  $g\tau=0.3, 0.5, 0.8$  given in Fig. 9(a). It can be seen that the probability drops at the transitions between the uncorrelated and correlated regimes as well as at the trapping. For  $g\tau=0.3$  (solid line) it decreases around  $k \cong 20$  due to the two-cavity trapping effect separating the stretched distribution into two regions. For  $g\tau=0.5$  (dashed line) it starts from a low level due to the coexistence of the uncorrelated and correlated regimes and then it drops again when the single-cavity trapping takes place at  $k \cong 40$ . The dot-dashed line for  $g\tau=0.8$  exhibits drops of the probability around  $k \cong 13$  at the transition between the uncorrelated and correlated regimes and around  $k \cong 33$  where the effect of the two trapping mechanisms becomes dominant. In order to generate the double-peaked superposition given in Fig. 9(a) first of all we have to follow the conditional measurement scheme  $a-M'M''-b$  and detect atoms always in their lower state after the interaction. This is made difficult especially by the dips in the probability curve. Furthermore, even if we measured the required sequence of atoms we have to shut the atomic beam down after the 30th atom, because the superposition would be destroyed by the atoms to come due to the trapping effects.

For large  $g\tau$ -s the distribution is bound in a dense lattice of single-cavity trapping lines as it can be seen in Fig. 11 for  $\alpha^2=30, g\tau=\pi$ . In this case the trapping lines are located around photon numbers of squares of integers mainly at 25, 36, and 49 corresponding to  $l=5, 6$ , and 7,

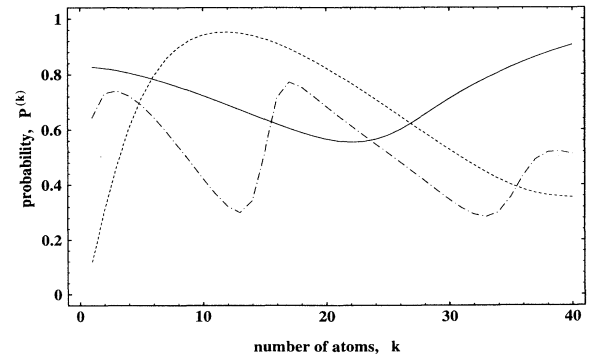


FIG. 10. The probabilities of detecting the lower state  $|b\rangle$  of atom number  $k$  in scheme  $a-M'M''-b$  during the evolution of the fields shown in Fig. 9(a) for  $g\tau=0.3, 0.5$ , and  $0.8$  depicted by the solid, dashed, and dot-dashed lines, respectively.

respectively, due to the  $\alpha^2=30$  initial fields in this example. This implies that the system reaches its trapping points after a few atoms very soon. In our example we get a lot of oscillatory structures above atom number  $k=6$  and the field depicted in Fig. 11 disappears.

Scheme  $b-M'M''-a$  is very similar to  $a-M'M''-b$  discussed above. The system experiences similar transitions between correlated and uncorrelated regimes, except the distribution evolves toward lower photon numbers, since in this scheme atoms are required to take a photon away from the fields. This also follows from the opposite shift of the amplitudes in Eq. (3.4d).

In this subsection we considered the two schemes,  $a-M'M''-b$  and  $b-M'M''-a$ , that do not preserve the energy of the system, which implies that stationary behavior cannot be achieved. The regular operation ends when the system runs into trapping points where the amplitude distribution is taken over by complicated rapidly oscillating structures. Nevertheless, in the regular regime before these structures would appear the system can exhibit correlated and uncorrelated regimes as well as transitions between them. In the correlated regime double-peaked photon statistics can be generated due to the effect of the coexisting single- and two-cavity trapping mechanisms. These fields showing high-order correlation seem to be difficult to produce in an experiment due to their transient character and the low detection probabilities of the conditioned atomic states. In the next subsection we are going to show that a combination of the energy-transferring and energy-preserving schemes can generate *arbitrary entangled steady states* of the two fields at reasonably high atomic detection probabilities.

### C. Combination of energy-transferring and energy-preserving schemes

It was shown in Sec. IV A that one can generate a set of Fock states located under the envelope of the initial

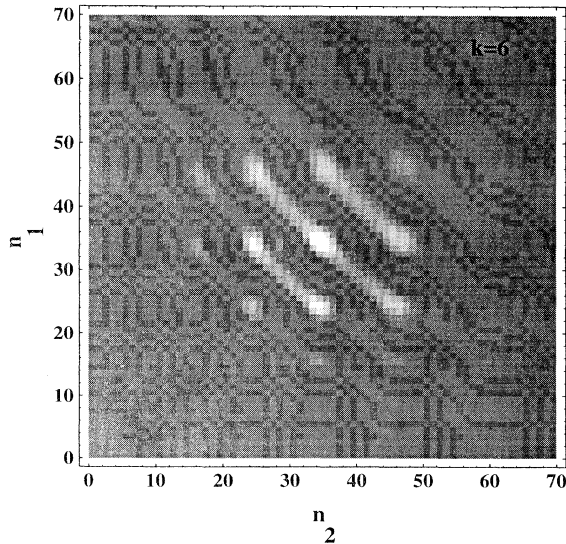


FIG. 11. Density plot of the amplitude distribution of the fields in scheme  $a-M'M''-b$  at atom number  $k=6$  for  $g\tau=\pi$  starting from coherent fields of parameter  $\alpha^2=30$ .

coherent states of the fields by the energy-preserving schemes, although they will be uncorrelated if the initial fields were uncorrelated. In Sec. IV B we learned that it is possible to generate correlated fields starting from uncorrelated ones by the energy-transferring schemes, although as a result of the trapping effects not at steady state. In the present section we want to combine these two kinds of schemes in such a way that after preparing a correlated state of fields from uncorrelated ones by energy-transferring schemes we use these correlated fields as initial condition and switch to an energy-preserving scheme. This way the generated Fock states will be located under the envelope of the “initial” correlated fields at steady state showing strong correlation between the two micromasers. Let us start the system in the scheme  $a-M'M''-b$  at interaction times such as  $g\tau=0.142$  from uncorrelated coherent fields of  $\alpha^2=30$ . It can be understood from Sec. IV B that after 100 atoms the generated fields will exhibit a long stretched distribution as depicted in Fig. 12(a) showing strong correlation between the fields. This correlation would be destroyed by the atoms to come due to the trapping mechanisms if scheme  $a-M'M''-b$  would be followed any further. We switch our system to another scheme instead. From  $k=101$  we continue in the energy-preserving scheme,  $a-M'M''-a$ , with altered interaction times, e.g., such as  $g\tau=\pi/2$ . The interaction time can be changed in an experiment by changing the velocity of the atoms. After the next 200 atoms we get a superposition of three Fock states at squares of even integers minus one depicted in Fig. 12(b) that could be approximated by

$$|\Psi\rangle \cong N(|99, 35\rangle + |63, 63\rangle + |35, 99\rangle), \quad (4.5)$$

where  $N$  is a normalization factor. This is also the steady state of the fields, since the production of the Fock states is a result of the same mechanism as the one discussed in Sec. IV A. In this case, however, the “initial” fields are correlated.

A “two-term” superposition of the fields can be produced if instead of  $\pi/2$  we choose  $g\tau=1.0$  to be the new interaction parameter. The generated fields are depicted in Fig. 12 (c) and can be approximated with

$$|\Psi\rangle \cong N(|88, 38\rangle + |38, 88\rangle) \quad (4.6)$$

showing 50th-order correlation at steady state. A three-dimensional plot of the photon probability distribution is given in Fig. 13 for this case. In Fig. 12(d) we show what happens if we switch between the schemes too early. Instead of  $k=100$  we make the same switch as above but now at  $k=50$ . Obviously, the distribution at the switch is much broader this time than it was in Fig. 12(a) allowing for a peak to arise at  $|38, 38\rangle$ .

The probability of finding the atoms in the desired states ( $|b\rangle$  before and  $|a\rangle$  after the switch) is depicted in Fig. 14. After getting through the risky first scheme,  $a-M'M''-b$ , and generating the stretched distribution for scheme  $a-M'M''-a$  to continue from, the detection of the conditioned atomic states becomes highly probable (unity at large  $k$ 's) locking the fields into a coherent superposition at steady state. In principle any superposition can be

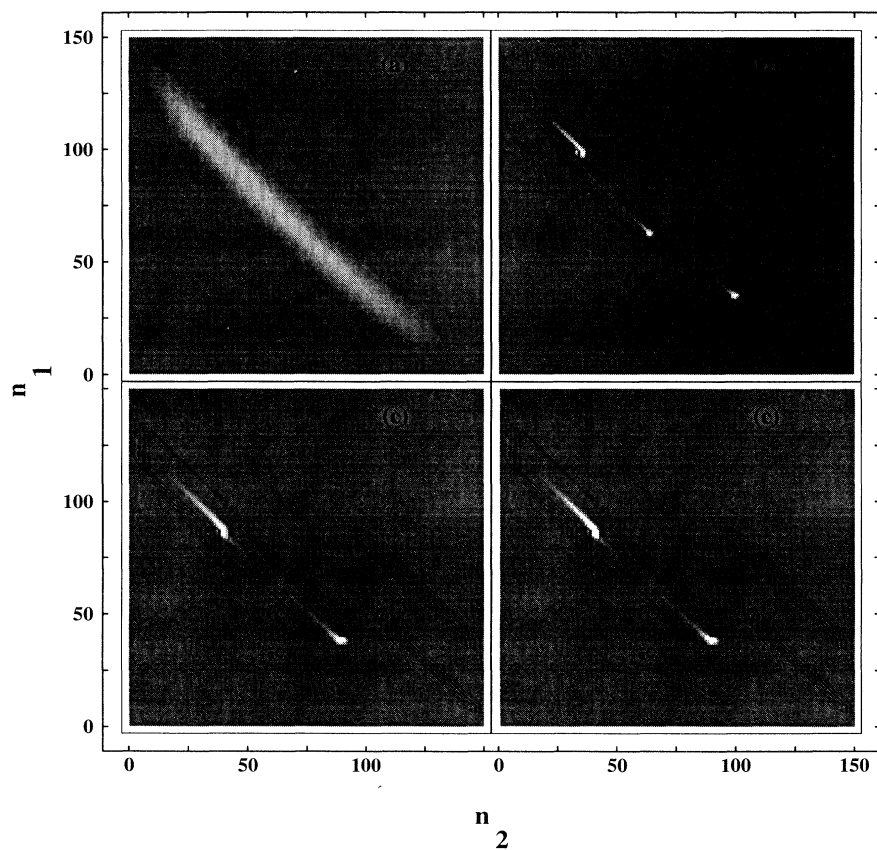


FIG. 12. Density plots of the amplitude distributions of the fields. (a) At the 100th atom starting from coherent fields of  $\alpha^2=30$  in scheme  $a-M'M''-b$  for  $g\tau=0.142$ ; (b) at the 300th atom after switching from the field generated in (a) at the 100th atom to  $a-M'M''-a$  for  $g\tau=\pi/2$ ; (c) same as (b) but switching to  $g\tau=1.0$ ; (d) same as (c) but switching at the 50th atom.

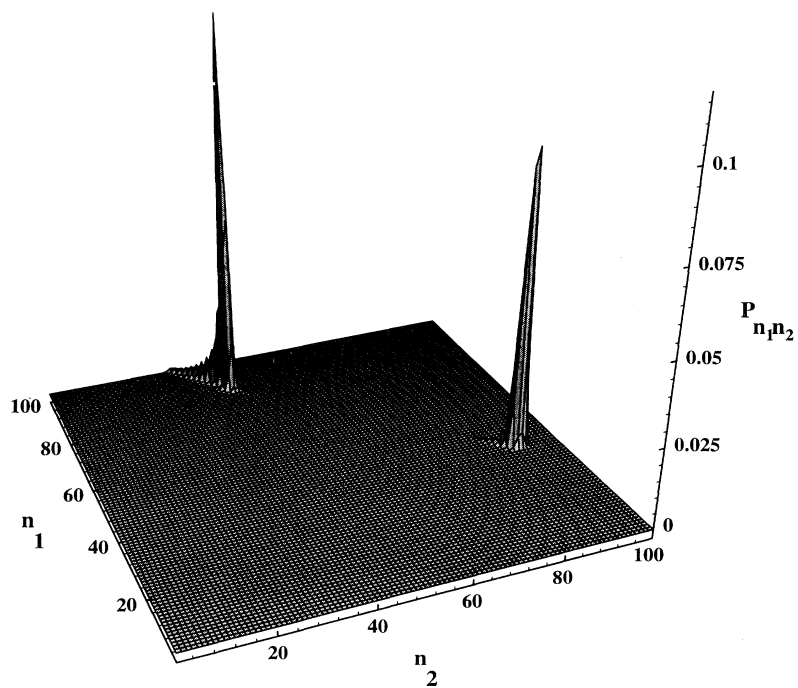


FIG. 13. Three-dimensional plot of the photon statistics that are the squares of the amplitudes depicted in Fig. 12(c) showing a double-peaked distribution at steady state.

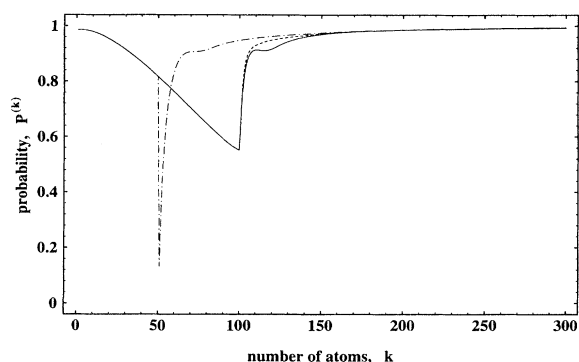


FIG. 14. Probabilities of detecting the required state of atom number  $k$  corresponding to the evolution of the fields in the schemes given in Fig. 12(b), 12(c), and 12(d) depicted by solid, dashed, and dot-dashed lines, respectively. The probability decreases before the switching, then after a transient at the switching it jumps to a high value and then increases to unity at steady state.

produced by choosing the appropriate initial coherent states and interaction parameters. The initial states set the region in the space,  $n_1 - n_2$ , where we are going to work. Using scheme  $a-M'M''-b$  the interaction parameters assure the production of a stretched distribution in this region provided  $g\tau\alpha = \pi/4$  is satisfied, and then in scheme  $a-M'M''-a$  they fix the location of the final Fock states under the envelope of the stretched distribution.

We should mention here, that stretched distributions can be generated by any of the two energy-transferring schemes, and any of the energy-preserving schemes can produce Fock states under the envelope of initial correlated fields. Thus, any pair of the energy-transferring and energy-preserving schemes can be used to produce a steady-state entanglement of nonlocal fields with considerably high detection probability.

## V. SUMMARY

In the present paper we studied two lossless micromasers coupled by the common pumping beam of two-level atoms when the state of the atoms is conditionally measured after the interaction. The atoms can follow two possible paths to reach the same final state the probabilities of which can be manipulated by the interaction times in the two cavities. The interference of two equally probable paths entangles the two fields while a single highly probable path results in two independent micromasers. Hence, the two fields can be correlated or decorrelated as we decide whether to favor two paths simultaneously or only one of them ("which-path" infor-

mation). This is very similar to Young's double slit experiment.

The pure evolution of the fields starting from uncorrelated coherent states is studied for the four simplest measurement schemes denoted by  $a-M'M''-a$ ,  $b-M'M''-b$ ,  $a-M'M''-b$ , and  $b-M'M''-a$  showing the state of the atoms,  $|a\rangle$  and  $|b\rangle$ , before and after the two maser cavities  $M'$  and  $M''$ . The energy-preserving schemes where all the atoms are injected before and detected after the interaction in the same state can be used to generate an uncorrelated set of Fock states in two dimensions under the envelope of the initial fields at steady state. We have very small transient entanglement of the two micromasers. The probability that the atoms follow the prescribed evolution scheme is high. It increases with atom number  $k$  and it is approximately unity for large  $k$ 's and at steady state.

In the case of the energy-transferring schemes the system is shown to operate in correlated or uncorrelated regimes or to make transitions between them depending on the interaction times. An entanglement of the fields resembling the two-term form of  $|N, N+M\rangle + |N+M, N\rangle$  of  $M$ th-order correlation can be achieved in the optimum case at a certain number of atoms as a result of the so-called single- and two-cavity trapping mechanisms. This entanglement is a transient effect, because further injection of atoms will destroy the superposition due to the trapping mechanisms themselves. The probability to detect atoms in the required lower state is low in these schemes and exhibits significant drops at the transitions between the correlated and the uncorrelated regimes as well as at the trapping points.

However, it is possible to generate an arbitrary steady-state entanglement of the fields with high detection probability by switching the system from an energy-transferring scheme to an energy-preserving one at an optimum atom number. The correlated state of fields generated by the former scheme serves as an initial condition for the latter one. This implies that the Fock states generated by the latter scheme will be located under the envelope of this amplitude distribution and the two nonlocal micromaser fields will be strongly correlated. In principle, arbitrary entanglement of macroscopically large number states of two nonlocal fields (nonlocal Schrödinger cat) can be achieved via this combination of schemes at steady state with high detection probability.

## ACKNOWLEDGMENTS

This research was supported by a grant from the Office of Naval Research, Grant No. N00014-92-J-1233, by a grant from the National Science Foundation, Grant No. PHY-9201912, and by a grant from the PSC-CUNY Research Award Program.

- [1] For a recent review, see H. Walther, Phys. Rep. **219**, 201 (1992); also H. Walther, Phys. Scr. **T23**, 165 (1988); F. Diedrich, J. Krause, G. Rempe, M. O. Scully, and H. Walther, IEEE J. Quantum Electron. **QE-24**, 1314 (1988).  
 [2] The experimental proof of the quantum collapse and re-

- vival predicted by the Jaynes-Cummings model was reported by G. Rempe, H. Walther, and N. Klein, Phys. Rev. Lett. **58**, 353 (1987).  
 [3] M. O. Scully and H. Walther, Phys. Rev. A **39**, 5229 (1989).

- [4] For the quantum theory of the micromaser, see P. Filipowicz, J. Javanainen, and P. Meystre, *Phys. Rev. A* **34**, 3077 (1986); the semiclassical theory is given by A. M. Guzman, P. Meystre, and E. W. Wright, *Phys. Rev. A* **40**, 2471 (1989).
- [5] L. A. Lugiato, M. O. Scully, and H. Walther, *Phys. Rev. A* **36**, 740 (1987).
- [6] L. Davidovich, J. M. Raimond, M. Brune, and S. Haroche, *Phys. Rev. A* **36**, 3771 (1987).
- [7] Quantum island states have been found in the micromaser by P. Bogár, J. A. Bergou, and M. Hillery, *Phys. Rev. A* **50**, 754 (1994); *Phys. Rev. A* (to be published).
- [8] H. Paul and T. Richter, *Opt. Commun.* **85**, 508 (1991).
- [9] P. Filipowicz, J. Javanainen, and P. Meystre, *Phys. Rev. A* **34**, 4547 (1986).
- [10] M. Brune, J. M. Raimond, and S. Haroche, *Phys. Rev. A* **35**, 154 (1987).
- [11] J. Krause, M. O. Scully, and H. Walther, *Phys. Rev. A* **36**, 4547 (1987).
- [12] P. Filipowicz, J. Javanainen, and P. Meystre, *J. Opt. Soc. Am. B* **3**, 906 (1986).
- [13] J. J. Slosser, P. Meystre, and S. L. Braunstein, *Phys. Rev. Lett.* **63**, 934 (1989).
- [14] P. Meystre, G. Rempe, and H. Walther, *Opt. Lett.* **13**, 1078 (1988).
- [15] J. J. Slosser and P. Meystre, *Phys. Rev. A* **41**, 3867 (1990).
- [16] J. J. Slosser, P. Meystre, and E. M. Wright, *Opt. Lett.* **15**, 233 (1990).
- [17] P. Meystre, J. Slosser, and M. Wilkens, *Phys. Rev. A* **43**, 4959 (1991).
- [18] The first masing in a single atom micromaser was reported by D. Meschede, H. Walther, and G. Müller, *Phys. Rev. Lett.* **54**, 551 (1985).
- [19] More recent results are reported by G. Rempe, F. Schmidt-Kaler, and H. Walther, *Phys. Rev. Lett.* **64**, 2783 (1990).
- [20] Superradiance in a micromaser cavity was first reported by J. M. Raimond, P. Goi, M. Gross, C. Fabre, and S. Haroche, *Phys. Rev. Lett.* **49**, 1924 (1982).
- [21] On the two-photon micromaser, see M. Brune, J. M. Raimond, P. Goy, L. Davidovich, and S. Haroche, *Phys. Rev. Lett.* **59**, 1899 (1987); and L. Davidovich, J. M. Raimond, M. Brune, and S. Haroche, *Phys. Rev. A* **36**, 3771 (1987).
- [22] See recent review on very high finesse cavities in the optical domain by S. E. Morino, Q. Wu, and T. W. Mossberg, *Opt. Photon. News* **3**, 8 (1992), and references therein. See also G. Rempe, R. J. Thompson, R. J. Brecha, W. D. Lee, and H. J. Kimble, *Phys. Rev. Lett.* **67**, 1727 (1991).
- [23] K. Vogel, V. M. Akulin, and W. P. Schleich, *Phys. Rev. Lett.* **71**, 1816 (1993).
- [24] P. Meystre and E. M. Wright, *Phys. Rev. A* **37**, 2524 (1988).
- [25] P. Meystre, *Opt. Lett.* **12**, 669 (1987).
- [26] J. A. Bergou and M. Hillery, *Phys. Rev. A* **44**, 7502 (1991).
- [27] Nonlocal microwave field quantum states have been found in a similar system by L. Davidovich, A. Maali, M. Brune, J. M. Raimond, and S. Haroche, *Phys. Rev. Lett.* **71**, 2360 (1993).
- [28] The production of entangled trapping states has been studied in the same system with nonselective measurements of the atomic states by P. Bogár and J. A. Bergou, *Phys. Rev. A* **51**, 2381 (1995). There, the fields are started from number states and the effects of dissipation and finite temperature are also investigated.
- [29] These schemes have also been investigated by V. Buzek, *Acta Phys. Slovaca* **44**, 1 (1994); V. Buzek and M. S. Kim, *J. Korean Phys. Soc.* **27**, 215 (1994).

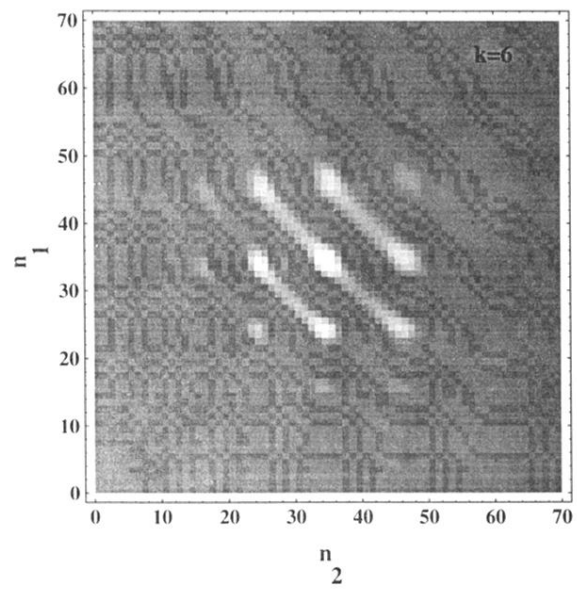


FIG. 11. Density plot of the amplitude distribution of the fields in scheme  $a-M'M''-b$  at atom number  $k=6$  for  $g\tau=\pi$  starting from coherent fields of parameter  $\alpha^2=30$ .

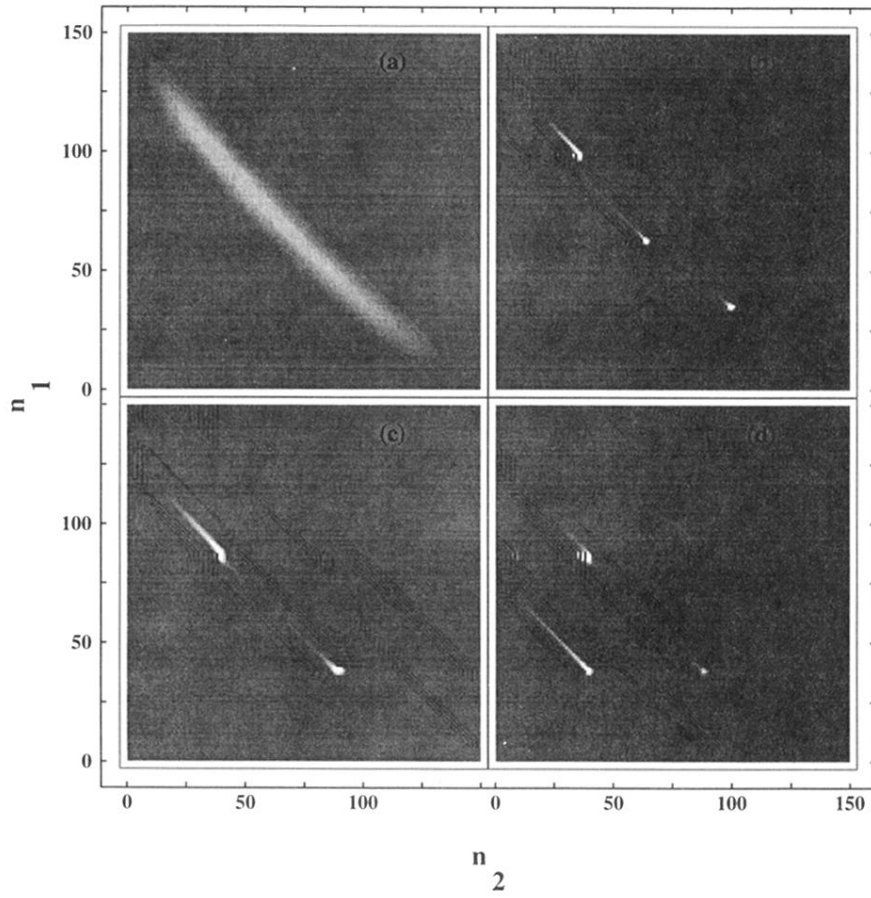


FIG. 12. Density plots of the amplitude distributions of the fields. (a) At the 100th atom starting from coherent fields of  $\alpha^2=30$  in scheme  $a-M'M''-b$  for  $g\tau=0.142$ ; (b) at the 300th atom after switching from the field generated in (a) at the 100th atom to  $a-M'M''-a$  for  $g\tau=\pi/2$ ; (c) same as (b) but switching to  $g\tau=1.0$ ; (d) same as (c) but switching at the 50th atom.

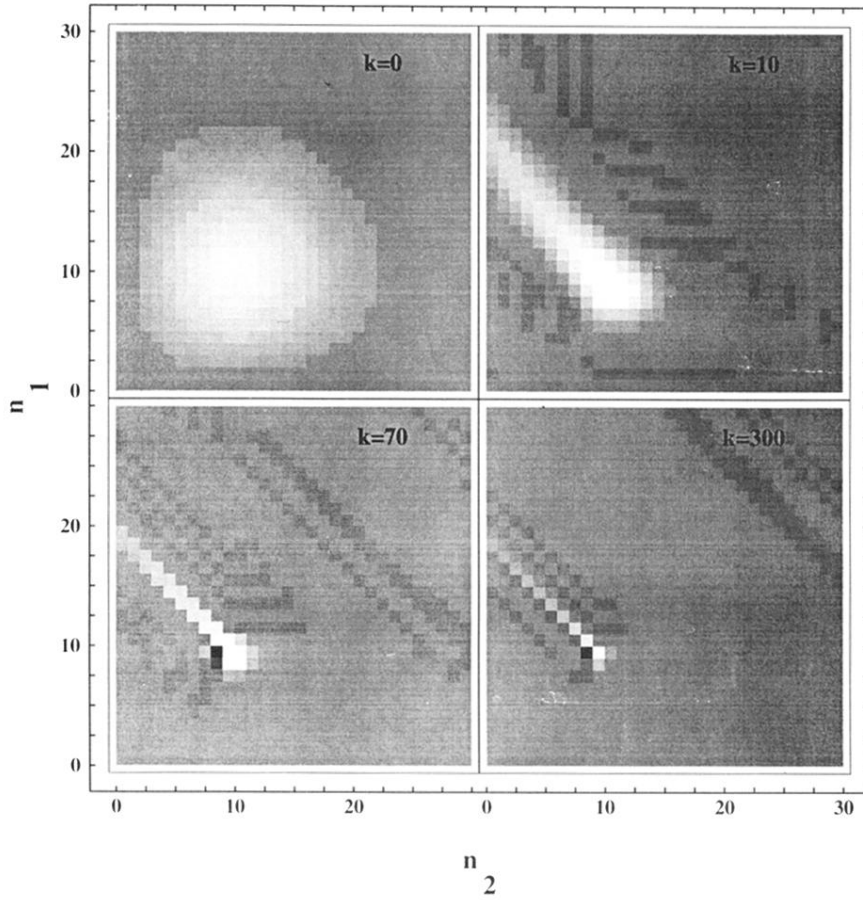


FIG. 5. Density plots showing the evolution of the amplitude distribution of the fields in the number representation in the case of scheme  $a-M'M''-a$ . Lighter and darker points indicate positive and negative amplitudes, respectively, as compared to the gray base of the zero level. The initial coherent field of parameter  $\alpha^2=10$  is given by the plot denoted by atom number  $k=0$ . The fields generated at  $g\tau=1.0$  for atom numbers  $k=10, 70$ , and  $300$  show a localization around the Fock state,  $|9,9\rangle$ , with small contributions from  $|10,8\rangle, |11,7\rangle, \dots, |18,0\rangle$  that are decreasing with  $k$ .

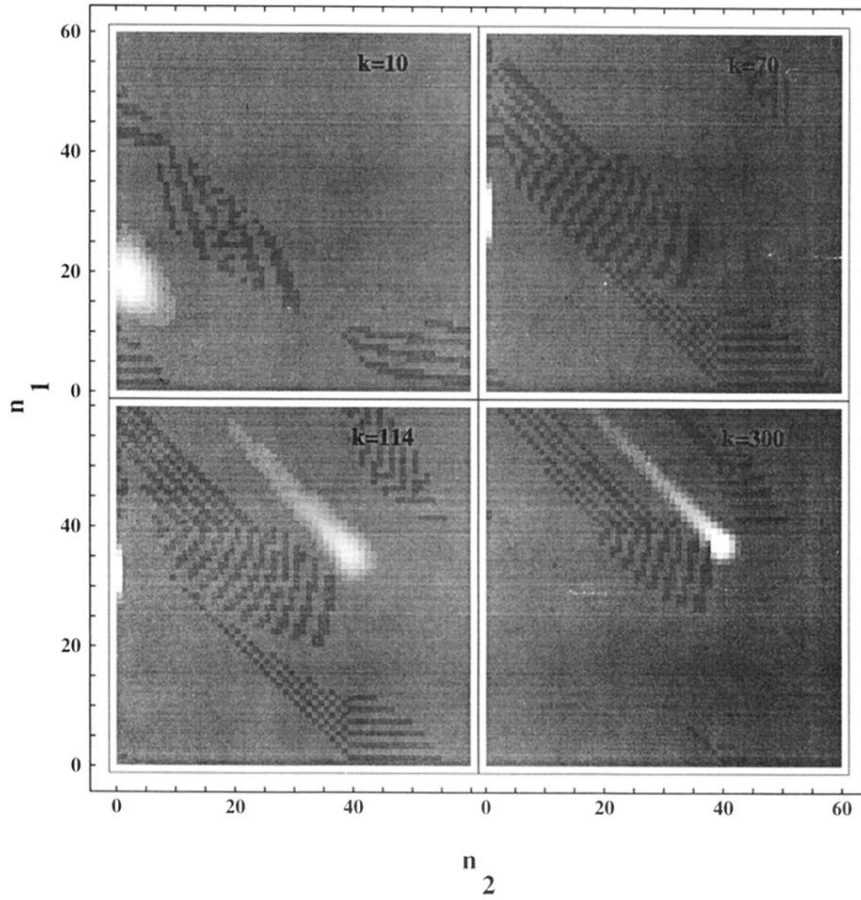


FIG. 6. Density plots showing the evolution of the amplitude distribution of the fields in scheme  $a-M'M''-a$  starting from the field shown in Fig. 5 for  $k=0$ . The generated fields at  $g\tau=0.5$  for atom numbers  $k=10, 70, 114,$  and  $300$  show a jump in the photon number in the second cavity around  $k=114$  and then a localization around the Fock state,  $|39,39\rangle$ , with small contributions from  $|40,38\rangle, |41,37\rangle, |42,36\rangle, \dots, |78,0\rangle$  that are decreasing with  $k$ .

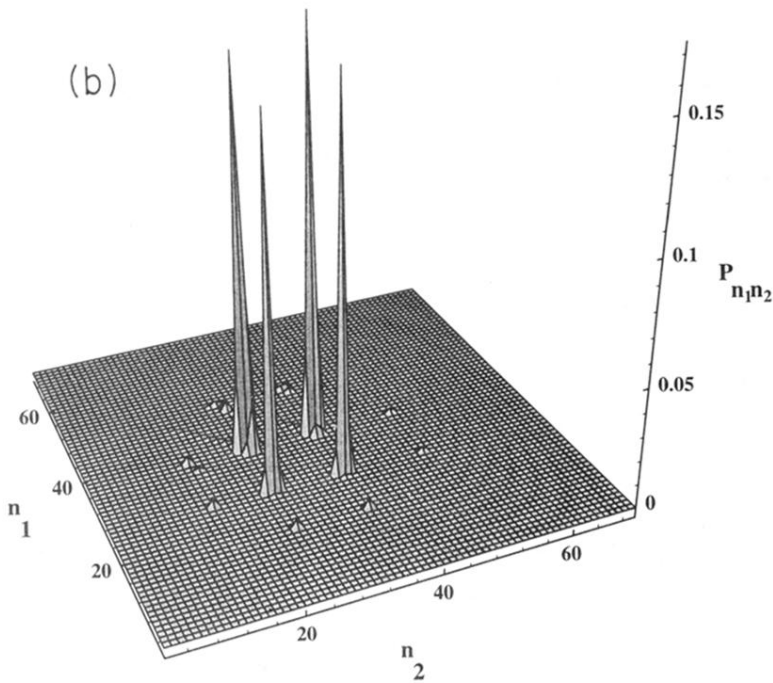
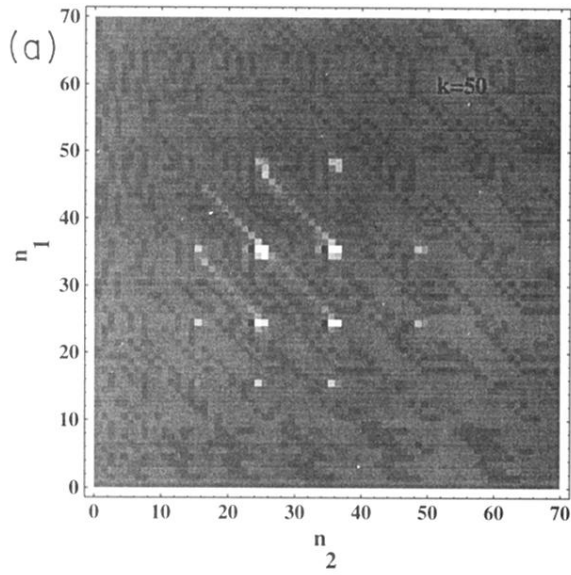


FIG. 8. (a) Density plot of the amplitude distribution of the fields in scheme  $a-M'M''-a$  at atom number  $k=50$  for  $g\tau=\pi$  starting from coherent fields of parameter  $\alpha^2=30$ . The generated Fock states are located at photon numbers that are squares integers minus one under the envelope of the amplitude distribution of the initial fields. (b) Three-dimensional plot of the photon statistics that are the squares of the amplitudes depicted in (a).

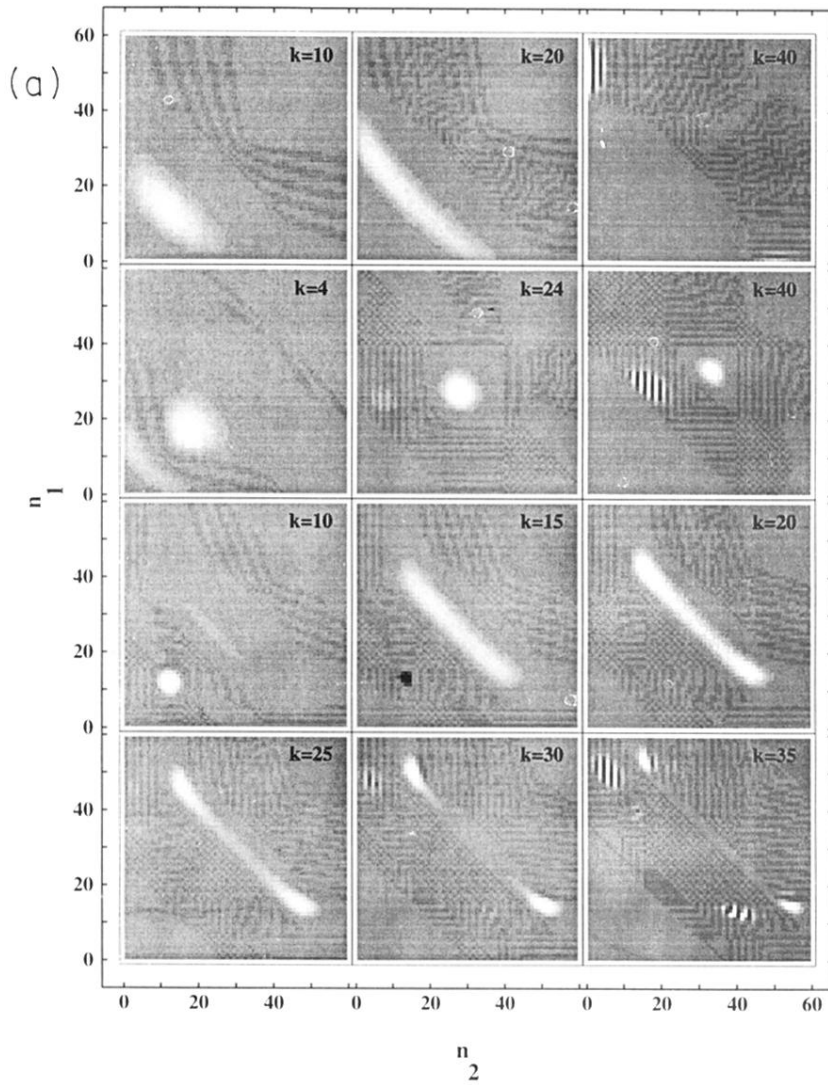


FIG. 9. (a) Density plots showing the evolution of the amplitude distribution of the fields in scheme  $a-M'M''-b$  starting from coherent fields depicted in Fig. 5 for  $k=0$ , where  $g\tau=0.3$  for the first, 0.5 for the second, and 0.8 for the third and fourth rows. The first and second rows represent the correlated and uncorrelated regimes, respectively, while a transition between these two regimes as well as a double-peaked distribution at  $k=30$  can be seen in the third and fourth ones. (b) Three-dimensional plot of the photon statistics that are the squares of the amplitudes depicted in (a) for  $g\tau=0.8$  at atom number  $k=30$  showing a double-peaked probability distribution.

